Soft Matter

Accepted Manuscript

This article can be cited before page numbers have been issued, to do this please use: W. Sokoowski, H. Jamil and K. Makuch, *Soft Matter*, 2026, DOI: 10.1039/D6SM00101G.

ROYAL SOCIETY OF CHEMISTRY

rsc.li/soft-matter-journal

View Article Online
DOI: 10.1039/D6SM00101G

Diffusion of rod-like particles in complex fluids

Władysław Sokołowski[1], Huma Jamil[1], and Karol Makuch*[1]

[1]Institute of Physical Chemistry, Polish Academy of Sciences, ul. Kasprzaka 44/52, 01-224 Warsaw, Poland

*Email: kmakuch@ichf.edu.pl

Abstract

Diffusion of particles in complex fluids and gels is difficult to describe and often lies beyond the scope of the classical Stokes-Einstein relation. One of the main lines of research over the past few decades has sought to relate diffusivity to a fundamental dissipative property of the fluid: the wave-vector-dependent shear viscosity function. Here, we use linear response theory to extend this viscosity function framework to rod-like particles. Using a dimer (two-bead particle) as a minimal rod-like probe, we derive explicit expressions for its diffusion coefficients parallel and perpendicular to its axis in terms of the viscosity function. We show that this description captures the full range of behaviors, from nearly isotropic diffusion of the rod-like probe to highly anisotropic, reptation-like motion. The method is based on a microscopic statistical-mechanical treatment of the Smoluchowski dynamics, yet leads to simple final formulas, providing a practical tool for interpreting diffusion experiments on rod-like tracers in complex fluids. We also clarify the limitations of this approach, emphasizing that the present formulation is primarily suited to complex liquids like polymer solutions, and only indirectly applicable to gels.

1 Introduction

Many macromolecules in nature possess a rod-like shape. This class includes actin filaments, microtubules, DNA fragments, certain viruses, cellulose fibers, and various synthetic nanorods[1–3]. In most of these cases, such rod-like particles exist in a liquid medium - either within the crowded interior of biological cells, which host thousands of molecular species, or in engineered environments such as liquid crystals used in industry[4].

Understanding macromolecular motion is thus of great practical and fundamental importance, particularly when the system is close to equilibrium. Even in the absence of external forces, a macromolecule is constantly jostled by surrounding atoms and molecules, causing its velocity to change direction repeatedly. At long times, this random motion becomes diffusive, with the mean-square displacement obeying $\left\langle [\mathbf{R}(t) - \mathbf{R}(0)]^2 \right\rangle = 6Dt$ which defines the diffusion coefficient D. The classical work of Sutherland, Einstein, and Smoluchowski established how this thermal motion is connected to dissipation. This result, known as the Einstein relation, $D = k_B T \mu$, relates the diffusion coefficient to the mobility μ measured from velocity response, $\mathbf{V} = \mu \mathbf{F}$, to a small applied force $\mathbf{F}$. In the Einstein formula, $k_B T$ is the Boltzmann constant and the absolute temperature. Because this relation follows from general principles of linear response theory, any systematic deviation in experiment or simulation indicates either a breakdown of equilibrium assumptions or an inconsistency in the methodology.

Einstein's relation thus provides a practical route for understanding diffusivity by studying the mobility of a probe subjected to a small force - the approach adopted in this work. Mobility quantifies the rate at which the work done by the applied force, $\mathbf{F} \cdot \mathbf{V} = \mathbf{F} \cdot \mu \mathbf{F}$, is dissipated in the surrounding fluid. A moving probe stores essentially no energy; instead, the energy input is continuously dissipated through viscous shear in the medium. Consequently, it is not surprising that the mobility of a spherical particle of radius a in a Newtonian fluid, $\mu = 1/6\pi\eta_0 a$, is determined by the fluid's shear viscosity η_0.

The dissipative (viscous) properties of a fluid can be probed by applying a sinusoidal volumetric force density acting on all fluid particles, $\mathbf{f}(\mathbf{r}) = f_0 \mathbf{e}_x \exp(-ik\mathbf{e}_z \cdot \mathbf{r})$. According to linear response theory, such forcing generates a velocity field of the same form, $\mathbf{v}(\mathbf{r}) = v_0 \mathbf{e}_x \exp(-ik\mathbf{e}_z \cdot \mathbf{r})$, with amplitude $v_0 = f_0/k^2\eta(k)$. The function $\eta(k)$, known as the wave-vector-dependent shear viscosity[5] is a fundamental property of any fluid[6]. This relation provides a general route for determining $\eta(k)$ in atomic, molecular, and complex fluids, including gels. For small wave-vectors $\eta(k)$ reduces to the macroscopic shear viscosity, $\eta_{\text{macro}} = \lim_{k\to 0} \eta(k)$. For simple molecular liquids, simulations show that $\eta(k)$ decreases with increasing k and approaches zero at wavelengths corresponding to only a few angstroms[7]. In contrast, the viscosity function of complex fluids has been explored far less[5,8]. In the context of Smoluchowski dynamics

View Article Online
DOI: 10.1039/D6SM00101G

- a coarse-grained description appropriate for colloidal suspensions and other macromolecular systems - $\eta(k)$ interpolates between the macroscopic viscosity at small wave-vectors, $\eta_{\text{macro}} = \lim_{k\to 0}\eta(k)$, and the solvent viscosity at large wave-vectors, $\eta_0 = \lim_{k\to\infty}\eta(k)$.

Linear response theory shows that the shear viscosity function also governs the velocity field generated by a localized perturbation, not only by a sinusoidal driving force. The average velocity field, $\langle \mathbf{v}(\mathbf{R})\rangle$, of an incompressible, homogeneous, and isotropic fluid subjected to a small point force $\mathbf{f}$ is given by[9]

$$\langle \mathbf{v}(\mathbf{R})\rangle = G_{\text{eff}}(\mathbf{R})\,\mathbf{f}, \tag{1}$$

where $G_{\text{eff}}(\mathbf{R})$ is called the effective Green function, and has the general Fourier-space form

$$\widehat{G}_{\text{eff}}(\mathbf{k}) = \frac{1}{k^2\eta(k)}\left(\mathbf{I} - \hat{\mathbf{k}}\hat{\mathbf{k}}\right), \tag{2}$$

explicitly involving the wave-vector-dependent viscosity $\eta(k)$. In practice, most numerical studies determine $\eta(k)$ either from equilibrium autocorrelation functions[10,11] or by applying a spatially sinusoidal force[12]. A convenient expression for the shear-viscosity function in terms of atomic degrees of freedom is given in Ref.[13]. The use of a point-force field, as in the expression above, to extract the viscosity function is rare. Experimental determinations of the viscosity function remain scarce. A recent approach proposes extracting $\eta(k)$ from measurements of the diffusion of probe particles with different hydrodynamic radii[14].

In general, the viscosity function depends on both wave vector and frequency, $\eta(k,\omega)$[6]. In our treatment, we focus on the long-time response, which corresponds to constant forcing of the fluid and, in the context of experiments on diffusion, observation of diffusivity at long times. Therefore, the response is considered in the zero-frequency limit, and $\eta(k,\omega)$ is replaced by $\eta(k,0)\equiv\eta(k)$.

Predictions for the shear-viscosity function - i.e., a viscosity that depends on wavelength and, in general, on frequency - are feasible for polymeric and other complex fluids, yet they remain relatively uncommon. In most cases, $\eta(k)$ appears as an auxiliary quantity within microscopic or generalized hydrodynamic descriptions, as in early treatments of polymer-solution viscosity[15], rather than as a central material function studied in its own right[8,16–19]. As a result, theoretical, numerical, and experimental determinations remain scarce, and a systematic assessment of the universal features of $\eta(k)$ is still timely.

On the theoretical side, kinetic and generalized hydrodynamic frameworks, such as the Hess and Doi theories for anisotropic (rod-like) macromolecules[20,21], provide a natural starting point. However, accessing genuine wave-vector dependence requires extending these approaches beyond spatially uniform flows to explicitly spatially varying velocity fields, so that the coupling between microstructural relaxation and flow gradients can be resolved as a function of length scale.

We argued above that the particle mobility is linked to the viscosity function $\eta(k)$. Determining the exact, general relation between them is, however, a difficult and still unsolved problem. This connection has been explored for spherical probes in two principal contexts: to understand deviations from the Stokes-Einstein relation in molecular liquids[22–24], and in such complex fluids as polymer melts[25] and colloidal suspensions in the limit where hydrodynamic effects are dominant[8]. Within Smoluchowski dynamics, the mobility can be related to $\eta(k)$, but direct interactions between the probe and surrounding macromolecules also contribute[14,26]. A complete statistical-physics treatment remains challenging and requires further development[9,26]. Existing analyses nevertheless provide simple phenomenological approximations that capture the orders-of-magnitude variation of diffusivity across different probe sizes, reflecting the hierarchy of length scales present in complex fluids. Comparable theoretical understanding is largely absent for nonspherical probes such as rod-like particles.

The diffusion of rod-like particles displays richer behavior than that of spheres. In simple Newtonian fluids, their mobility is anisotropic: motion along the rod's axis is easier than motion perpendicular to it. The mobility ratio $\mu_\parallel/\mu_\perp$ exceeds unity and depends logarithmically on the aspect ratio $p = L/d$ (length to diameter). In the large-p limit, one finds $\mu_\parallel/\mu_\perp = 1 + 0.09/\log p$[27]. For very slender rods, the difference between longitudinal and transverse mobility becomes small, and the center-of-mass diffusion becomes isotropic. In contrast, rod diffusion in dense polymer melts exhibits the opposite trend: $\mu_\parallel/\mu_\perp$ increases strongly with p indicating a pronounced suppression of transverse motion[28]. In this regime, rods predominantly translate along their long axis while lateral displacements are strongly hindered - a behavior reminiscent of reptation dynamics originally introduced for motion between immobile obstacles[29].

In this paper, we ask whether the viscosity function $\eta(k)$ can also capture the rich dynamical behavior of rod-like particles in complex fluids. Because the diffusion of many nonspherical, rod-like particles, including DNA oligomers[30], is well described by modeling the particles as agglomerates of beads[31], we begin our investigation of the relation between the viscosity function and the diffusion of nonspherical, rod-like particles by focusing on a dimer - the simplest model of a rod-like particle.

We compute the mobility of a dimer by assuming that the dominant hydrodynamic contribution arises from the coupling of its two beads through the effective Green function $G_{\text{eff}}(\mathbf{R})$ (point-force coupling). This approach follows recent statistical-physics developments for complex fluids[9,14]. Under this assumption, we obtain a simple approximation reminiscent of Smoluchowski's original treatment of two interacting spheres, yielding explicit expressions for the parallel and perpendicular mobilities

View Article Online
DOI: 10.1039/D6SM00101G

of the dimer in terms of the viscosity function and the hydrodynamic radii of its constituent beads.

This framework allows us to evaluate how a wave-vector-dependent viscosity influences the anisotropic motion of a rod-like probe. Remarkably, different forms of $\eta(k)$ naturally reproduce both spherical-like behavior in simple fluids and reptation-like dynamics in crowded environments.

A key strength of this approach is that it relies solely on the viscosity function - a fundamental property of any fluid - without invoking system-specific microscopic details[32] or phenomenological fitting parameters[33]. In contrast to numerical simulations that proceed directly from a model system to its diffusivity[34], our method highlights the role of $\eta(k)$ as the underlying physical quantity controlling mobility.

2 Mobility

To provide background for our discussion of diffusion in complex fluids, we first consider the motion of two non-Brownian spheres in a simple fluid. In a simple incompressible Newtonian fluid, the mobility of a dumbbell can be formulated in terms of the classical two-body mobility problem discussed by Smoluchowski[35]. Consider two identical spherical beads of radius a, centered at positions $\mathbf{R}_1$ and $\mathbf{R}_2$, and immersed in a fluid of shear viscosity η_0. In the Stokes regime, the translational velocities depend linearly on the applied forces,

$$\mathbf{V}_i = \sum_{j=1}^{2} \boldsymbol{\mu}_{ij}(\mathbf{R})\,\mathbf{F}_j, \qquad \mathbf{R} = \mathbf{R}_2 - \mathbf{R}_1, \tag{3}$$

where $\boldsymbol{\mu}_{ij}$ is the two-particle mobility matrix[36].

This is the standard hydrodynamic mobility problem for two spheres, already underlying Smoluchowski's analysis of sedimenting particles. For identical beads, symmetry implies, $\boldsymbol{\mu}_{11} = \boldsymbol{\mu}_{22}$, and $\boldsymbol{\mu}_{12} = \boldsymbol{\mu}_{21}$. At large (infinite) separations, the self-mobility reduces to the Stokes value,

$$\boldsymbol{\mu}_{11} \approx \mu_0 \mathbf{I}, \qquad \mu_0 = \frac{1}{6\pi\eta_0 a}. \tag{4}$$

At finite but large separation, a flow generated by one bead is felt by the other. Thus, in particular, two spheres sedimenting in a gravitational field influence each other's motion through the fluid. This influence is called hydrodynamic interaction and is encoded in the mobility matrix. At large separations, the hydrodynamic interaction between the two beads is given, to leading order, by the Oseen tensor,

$$\boldsymbol{\mu}_{12}(\mathbf{R}) \approx \mathbf{G}_0(\mathbf{R}) = \frac{1}{8\pi\eta_0 R}\left(\mathbf{I} + \hat{\mathbf{R}}\hat{\mathbf{R}}\right). \tag{5}$$

A more accurate description, valid up to $1/R^3$, is obtained by replacing the Oseen pair mobility with the finite-size Rotne-Prager tensor[37]. For two identical non-overlapping spheres, $R \geq 2a$,

$$\boldsymbol{\mu}_{12}^{\mathrm{RP}}(\mathbf{R}) = \frac{1}{8\pi\eta_0 R}\left[\left(1 + \frac{2a^2}{3R^2}\right)\mathbf{I} + \left(1 - \frac{2a^2}{R^2}\right)\hat{\mathbf{R}}\hat{\mathbf{R}}\right]. \tag{6}$$

The dumbbell mobility follows directly from this two-body problem. If the total external force $\mathbf{F}_{\mathrm{tot}}$ is distributed equally between the two beads, $\mathbf{F}_1 = \mathbf{F}_2 = \mathbf{F}_{\mathrm{tot}}/2$, the two velocities are identical, $\mathbf{V}_1 = \mathbf{V}_2$. Then the center-of-mass velocity is

$$\mathbf{V} = \frac{\mathbf{V}_1 + \mathbf{V}_2}{2} = \frac{1}{2}\left(\boldsymbol{\mu}_{11} + \boldsymbol{\mu}_{12}\right)\mathbf{F}_{\mathrm{tot}}. \tag{7}$$

The dumbbell mobility matrix is defined by

$$\mathbf{V} = \mathbf{M}\left(\mathbf{R}\right)\mathbf{F}_{\mathrm{total}}. \tag{8}$$

with

$$\mathbf{M}(\mathbf{R}) = \frac{1}{2}\left(\boldsymbol{\mu}_{11}(\mathbf{R}) + \boldsymbol{\mu}_{12}(\mathbf{R})\right). \tag{9}$$

At the Oseen level, the dumbbell mobility matrix becomes

$$\mathbf{M}(\mathbf{R}) \approx \frac{1}{2}\mu_0\mathbf{I} + \frac{1}{2}\mathbf{G}_0(\mathbf{R}), \tag{10}$$

while at the Rotne-Prager level, $\mathbf{M}(\mathbf{R}) \approx \frac{1}{2}\mu_0\mathbf{I} + \frac{1}{2}\boldsymbol{\mu}_{12}^{\mathrm{RP}}(\mathbf{R})$.

Decomposing $\mathbf{M}(\mathbf{R})$ into components parallel and perpendicular to the dumbbell axis,

$$\mathbf{M}\left(\mathbf{R}\right) = \mu_{\parallel}\left(R\right)\,\hat{\mathbf{R}}\hat{\mathbf{R}} + \mu_{\perp}\left(R\right)\left(\mathbf{I} - \hat{\mathbf{R}}\hat{\mathbf{R}}\right), \tag{11}$$

one finds

$$\mu_{\parallel}(R) \approx \frac{1}{2}\mu_0 + \frac{1}{8\pi\eta_0 R}, \qquad \mu_{\perp}(R) \approx \frac{1}{2}\mu_0 + \frac{1}{16\pi\eta_0 R}, \tag{12}$$

in the leading-order far-field approximation. Hence, the parallel mobility exceeds the perpendicular one, reflecting the anisotropic hydrodynamic coupling generated by two-body Stokes flow. The Rotne-Prager correction yields

$$\mu_{\parallel}(R) \approx \frac{1}{12\pi\eta_0 a} + \frac{1}{8\pi\eta_0 R}\left(1 - \frac{2a^2}{3R^2}\right), \tag{13}$$

and

$$\mu_{\perp}(R) \approx \frac{1}{12\pi\eta_0 a} + \frac{1}{16\pi\eta_0 R}\left(1 + \frac{2a^2}{3R^2}\right). \tag{14}$$

The Rotne-Prager correction therefore provides the leading finite-size improvement to the Smoluchowski-Oseen picture. At still shorter separations, when $R \approx 2a$, lubrication forces become important, and neither the Oseen nor the Rotne-Prager form is sufficient; one must then use the exact two-sphere mobility functions[36].

One inspiration for our paper is expression (10) for the dumbbell mobility in the far-field approximation, which

View Article Online
DOI: 10.1039/D6SM00101G

is composed of the mobility of a single bead and the far-field (Oseen) hydrodynamic coupling. This expression contains a single-bead contribution and the Oseen tensor, which describes the hydrodynamic velocity field in an incompressible simple fluid generated by a small point force. For incompressible complex fluids, we expect the same structure for a dumbbell: the two-body mobility matrix of a dumbbell immersed in a complex fluid is given by an infinite-separation contribution, μ_{single}, and a far-field contribution given by the effective Green function,

$$\mathbf{M}(\mathbf{R}) \approx \frac{1}{2}\mu_{\text{single}}\mathbf{1} + \frac{1}{2}G_{\text{eff}}(\mathbf{R}). \tag{15}$$

Another inspiration for the above formula comes from microscopic statistical-physics reasoning, which deserves a separate paper. Here, in the rest of this section, we sketch the underlying logic and provide heuristic reasoning. In many experiments, rod-like particles are tracked by monitoring their motion at fixed orientation [38]. The parallel and perpendicular components of mobility then provide valuable insight into the surrounding medium. To mimic this situation, we consider a rod-like particle with fixed orientation and model it as an oriented dumbbell. Because the surrounding complex fluid is statistically isotropic, the mobility matrix is also isotropic and can therefore be decomposed as in Eq. (11). The coefficients $\mu_{\parallel}$ and $\mu_{\perp}$ are influenced by many effects, including how the presence of the dumbbell perturbs the otherwise isotropic complex fluid through direct, hydrodynamic, and other interactions present in the system.

For sufficiently large bead separations, hydrodynamic coupling between the beads becomes negligible. In this limit, the dumbbell behaves as two independent particles constrained to move together, and its center-of-mass mobility is simply one-half of the single-bead mobility, $\mu_{\parallel}(R) = \mu_{\perp}(R) = \mu_{\text{single}}/2$. It gives the first of the terms in approximation (15).

To analyze $\mu_{\parallel}$ and $\mu_{\perp}$ in more detail, we work within Smoluchowski dynamics, which provides a coarse-grained description of macromolecules in solution [39]. Unlike molecular dynamics, Smoluchowski dynamics averages over the solvent degrees of freedom, leaving only the positional degrees of freedom of the macromolecules. These undergo Brownian motion under both direct interactions and hydrodynamic interactions mediated by the solvent.

As for the case of simple fluids described above, we analyze the parallel and perpendicular mobilities of a dumbbell through the lens of the effective two-particle mobility matrix. This matrix arises naturally when considering the motion of macromolecules subjected to a small external force. A force $\mathbf{F}_1$ applied to particles at position $\mathbf{R}_1$, sets the entire complex fluid into motion, including nearby macromolecules. For sufficiently small forces, the average velocity response of particles at a second position, $\mathbf{R}_2$, is linear,

$$\mathbf{V}_2 = \mu_{21}^{\text{eff}}(\mathbf{R}_2 - \mathbf{R}_1)\mathbf{F}_1,$$

where $\mu_{21}^{\text{eff}}(\mathbf{R})$ is the effective pair mobility. Likewise, the particles on which the force acts respond linearly,

$$\mathbf{V}_1 = \mu_{\text{self}}^{\text{eff}}\mathbf{F}_1,$$

with $\mu_{\text{self}}^{\text{eff}}$ the effective self-mobility matrix [9].

It is not ultimately clear to us, to what extent the two problems: effective two-particle mobility in complex fluid and the mobility matrix of the dumbbell are related. This topic deserves further study, which is beyond the scope of this paper.

The effective mobility matrices described above have been analyzed in various contexts within Smoluchowski dynamics. However, deriving fully microscopic expressions for these quantities remains challenging [9,26]. What is known is that the effective pair mobility of two particles has the following Fourier-space structure, $\hat{\mu}_{12}^{\text{eff}}(\mathbf{k}) = \hat{\mu}_{12}^{\text{irr}}(\mathbf{k}) + \hat{\mu}_{<}^{\text{irr}}(\mathbf{k})\, G_{\text{eff}}(\mathbf{k})\, \hat{\mu}_{>}^{\text{irr}}(\mathbf{k})$ [9]. This relation provides a clear example of how a macroscopic transport quantity - here, the effective pair mobility $\hat{\mu}_{12}^{\text{eff}}(\mathbf{k})$ - naturally incorporates the viscosity function through G_{eff}. We do not examine the details of the matrices $\hat{\mu}_{12}^{\text{irr}}(\mathbf{k})$, $\hat{\mu}_{<}^{\text{irr}}(\mathbf{k})$ and $\hat{\mu}_{>}^{\text{irr}}(\mathbf{k})$, it is sufficient to note that the "irr" terms are expected to be short-ranged, decaying faster than $1/R^3$ for large R in real space for Stokes flow [40], and that $\hat{\mu}_{>,<}^{\text{irr}}(\mathbf{k})$ reduce to the identity matrix as $\mathbf{k} \to 0$ [26]. Under these conditions, the long-distance behavior of the effective pair mobility simplifies to

$$\mu_{12}^{\text{eff}}(\mathbf{R}) \approx G_{\text{eff}}(\mathbf{R}), \tag{16}$$

where $\mathbf{G}_{\text{eff}}(\mathbf{R})$ is the effective Green tensor. This mirrors Smoluchowski's result for two sedimenting spheres, where hydrodynamic interactions at large separations were captured by the bare Oseen tensor, $\mu_{12}^{\text{eff}}(\mathbf{R}) \approx G_0(\mathbf{R})$ [35].

We use the above "point-force coupling" to describe how the beads in an oriented dumbbell influence each other's motion in the mobility problem. A force $\mathbf{F}_2$ acting on bead 2 generates a hydrodynamic flow field $G_{\text{eff}}(\mathbf{R})\mathbf{F}_2$ at the position of bead 1. Applying the same force to bead 1, $\mathbf{F}_1 = \mathbf{F}_2 = \mathbf{F}_{\text{total}}/2$, produces an analogous contribution. Combining these effects yields the "point-force coupling" approximation for the dumbbell mobility matrix given by Eq. (15), which reduces to Eq. (10) for a simple fluid. We have already seen that this approximation for a simple fluid is a leading, far field contribution, for which the correction comes from the Rotne-Prager term, as in Eq. (6). This points to the limit, in which we expect the approximation (15) to work.

The expression for the dumbbell mobility matrix given by Eq. (15) constitutes the main approximation scheme introduced in this work. It requires only two ingredients: the single-bead mobility matrix and the viscosity function $\eta(k)$, which enters through the effective Green function $G_{\text{eff}}(\mathbf{k})$ defined in Eq. (2).

View Article Online
DOI: 10.1039/D6SM00101G

Further limitations of the approximation in Eq. (15) ultimately reduce to determining under which conditions the exact fixed-orientation dumbbell mobility indeed simplifies to this form. This question can be addressed directly in numerical simulations, since the approximation depends only on the single-bead mobility and the viscosity function. A complementary route is to analyze the problem using rigorous statistical-physics methods. Guided by earlier work[9,14,26,41], we expect the exact mobility of a dumbbell to have the structure, $\mathbf{M}(\mathbf{R}) = \mu_{11}^{\mathrm{dl}}(\mathbf{R}) + \mu_{12}^{\mathrm{dl}}(\mathbf{R})$ with $\hat{\mu}_{12}^{\mathrm{dl}}(\mathbf{k}) = \hat{\mu}_{12}^{\mathrm{dl,irr}}(\mathbf{k}) + \hat{\mu}_{<}^{\mathrm{dl,irr}}(\mathbf{k})\, G_{\mathrm{eff}}(\mathbf{k})\, \hat{\mu}_{>}^{\mathrm{dl,irr}}(\mathbf{k})$ with the viscosity function entering via G_{eff} and the properties analogous to μ^{irr} matrices discussed above for effective pair mobility. Current understanding[26] indicates that direct interactions between the dumbbell and surrounding macromolecules of a complex fluid can significantly influence the range of the $\mu^{\mathrm{dl,irr}}(\mathbf{R})$.

Nevertheless, when the beads neither adhere to nearby macromolecules nor strongly perturb their structure through long-range repulsion, we anticipate that Eq. (15) provides a reliable approximation for the dumbbell mobility. Such conditions exclude situations involving caging or trapping of probes in gels.

3 Wave-vector-dependent viscosity, $\eta(k)$

One of the two essential components of the approximation given by Eq. (15) is the effective Green function from Eq. (2). Its inverse Fourier transform to position space yields,

$$G_{\mathrm{eff}}(\mathbf{R}) = \phi(R)\,\mathbf{I} + \psi(R)\left(\mathbf{I} - 3\hat{\mathbf{R}}\hat{\mathbf{R}}\right), \tag{17}$$

with two scalar functions $\phi(R)$ and $\psi(R)$,

$$\phi(R) = \frac{1}{3\pi^2}\int_0^\infty \frac{j_0(kR)}{\eta(k)}dk, \tag{18}$$

$$\psi(R) = -\frac{1}{6\pi^2}\int_0^\infty \frac{j_2(kR)\,dk}{\eta(k)}, \tag{19}$$

where $j_0(kR) = \sin(kR)/kR$ and $j_2(kR) = \left(\frac{3}{(kR)^3} - \frac{1}{kR}\right)\sin(kR) - \frac{3}{(kR)^2}\cos(kR)$ are spherical Bessel functions. From incompressibility, together with the conditions $\lim_{R\to 0}\phi(R)R^3 = \lim_{R\to 0}\psi(R)R^3 = 0$, one obtains the following relation between these scalar functions,

$$\psi(R) = \frac{1}{2}\phi(R) - \frac{3}{2R^3}\int_0^R s^2\phi(s)\,ds. \tag{20}$$

A prototypical example of a complex fluid is a suspension of spherical particles, in which the viscosity function equals the macroscopic viscosity at $k = 0$ and decreases with k approaching the solvent viscosity η_0[8]. To model this behavior, we introduce the phenomenological form

$$\eta(k) = \eta_{\mathrm{macro}}\frac{1 + (\lambda k)^2}{1 + \frac{\eta_{\mathrm{macro}}}{\eta_0}(\lambda k)^2}, \tag{21}$$

which contains the parameters η_{macro}, η_0, and λ, interpreted as the macroscopic viscosity, the solvent viscosity, and a length scale governing the crossover from η_{macro} to η_0. We emphasize that Eq. (21) describes only the complex fluid and is independent of dimer (probe-particle) properties. Moreover, the viscosity function depends only on the magnitude of the wave vector, which reflects the isotropy of the complex fluid in which the dumbbell is immersed. There is only one length scale, λ, that characterizes the complex fluid; this is not the case for $\eta(k)$ in aqueous poly(ethylene glycol) solutions, which we consider later. The advantage of the form in Eq. (21) is that substituting it into Eqs. (18) and (19) yields explicit expressions for the scalar functions in the effective Green function:

$$\phi(R) = \frac{1}{6\pi\eta_{\mathrm{macro}}R}\left[1 + \left(\frac{\eta_{\mathrm{macro}}}{\eta_0} - 1\right)\exp\left(-\frac{R}{\lambda}\right)\right], \tag{22}$$

$$\psi(R) = -\frac{1}{12\pi\eta_{\mathrm{macro}}}\left[\left(\frac{\eta_{\mathrm{macro}}}{\eta_0} - 1\right)\frac{3\lambda^2}{R^3} + \frac{1}{2R} - \left(\frac{\eta_{\mathrm{macro}}}{\eta_0} - 1\right)\left(\frac{1}{R} + \frac{3\lambda}{R^2} + \frac{3\lambda^2}{R^3}\right)\exp\left(-\frac{R}{\lambda}\right)\right]. \tag{23}$$

In the special case where the macroscopic shear viscosity equals the solvent viscosity, $\eta_{\mathrm{macro}} = \eta_0$, the effective Green function reduces to the Oseen tensor $G_0(\mathbf{R}) = \left(\mathbf{I} + \hat{\mathbf{R}}\hat{\mathbf{R}}\right)/8\pi\eta_0 R$[42]. Since $\mathbf{f}\cdot G_0(\mathbf{R})\cdot\mathbf{f} > 0$ for all $\mathbf{R}$, a downward force induces a downward motion of the fluid everywhere (although the velocity need not be parallel to the force). We observe qualitatively similar behavior in a complex fluid with a modest viscosity contrast, for example, $\eta_{\mathrm{macro}}/\eta_0 = 5$ and $\lambda = 10^{-7}$m, as shown in Fig. 1(a). However, increasing the viscosity ratio $\eta_{\mathrm{macro}}/\eta_0$ leads to regions where the local flow reverses direction relative to the applied force, as illustrated in 1(b) for $\eta_{\mathrm{macro}}/\eta_0 = 48$ and $\lambda = 10^{-7}$m. The corresponding velocity field exhibits vortex-like structures around these regions of reversed flow, reminiscent of similar "vortices" reported in porous media[43]. In a porous medium, static obstacles may impede the fluid from establishing a coherent, co-directed motion ahead of the forcing point. As a consequence, the velocity field is screened, and the response exhibits localized recirculating flow structures. By analogy, a complex fluid can act as an effective porous matrix: near the point force, the flow is essentially solvent-like, with the usual Oseen scaling $\sim 1/(r\,\eta_0)$, whereas at larger distances the response crosses over to a weaker flow, $\sim 1/(r\,\eta_{\mathrm{macro}})$, governed by the macroscopic viscosity. This crossover can

View Article Online
DOI: 10.1039/D6SM00101G

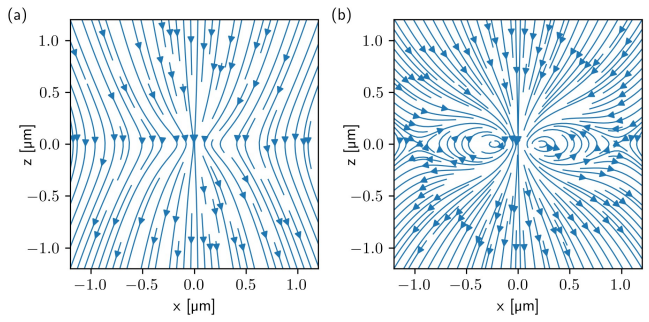

Figure 1: Streamlines of the velocity fields from Eq. (1) generated by a point force $\mathbf{f} = -10^{-12}\hat{\mathbf{z}}\,\mathrm{N}$ with the viscosity function given by Eq. (21) for: (a) length $\lambda = 10^{-7}\mathrm{m}$, viscosity ratio $\eta_{\mathrm{macro}}/\eta_0 = 5$; (b) length $\lambda = 10^{-7}\mathrm{m}$, viscosity ratio $\eta_{\mathrm{macro}}/\eta_0 = 48$.

be interpreted as an emergent obstruction to long-range velocity field, producing "vortex-like" or recirculating features reminiscent of flows in porous media. This comparison is only qualitative, however, because the far-field asymptotics of the Green function in complex fluids generally differ from those in porous media and in gels with an immobile component.

4 Application

Using Eq. (17) in the approximation (15) and identifying the mobility coefficient through the definition (11) we obtain

$$\mu_{\parallel} = \frac{1}{2}\left[\mu_{\mathrm{single}}(a) + \phi(R) - 2\psi(R)\right], \tag{24}$$

$$\mu_{\perp} = \frac{1}{2}\left[\mu_{\mathrm{single}}(a) + \phi(R) + \psi(R)\right]. \tag{25}$$

These expressions constitute a simple methodology for determining the dumbbell mobilities directly from the single-bead mobility μ_{single} and the viscosity function $\eta(k)$ (equivalently, from the scalar functions $\phi(R)$ and $\psi(R)$). The difference between the above mobility coefficients is,

$$\mu_{\parallel} - \mu_{\perp} = -\frac{3}{2}\psi(R). \tag{26}$$

Eqs. (24-26) suggest several tests of the proposed theory. The most straightforward test is to experimentally determine all four quantities from Eq. (24). This requires first determining the components of the effective Green function, $\phi(R)$ and $\psi(R)$, which depend solely on the properties of the complex fluid and not on the dimer. This step is already very challenging: with only a few exceptions, the effective Green function is not used to describe flow in complex fluids. The viscosity function is more commonly used in descriptions of simple fluids in numerical simulations, but it is difficult to calculate theoretically for complex fluids[8,44]. As a result, much experimental work on particle diffusion is left without interpretation, in contrast to diffusion experiments in simple fluids, which can be interpreted via the Stokes-Einstein equation based on viscosity. There have been only limited attempts to generalize the Stokes-Einstein relation to the shear-viscosity function[8,14,22–25,44]. Because of this limited interest in the shear-viscosity function, there is a need for a better understanding and characterization of shear viscosity as a function of wave vector in the zero-frequency limit.

A second difficulty in finding experimental data lies in the fact that some rod-like particles cannot be represented by a dumbbell: from the perspective of Stokes equations with stick boundary conditions, a dumbbell made of two beads is characterized solely by the aspect ratio L/a. Varying this parameter offers only limited control over the hydrodynamic anisotropy, $\mu_{\parallel}/\mu_{\perp}$, and therefore provides a restricted basis for quantitatively interpreting measurements on rod-like phages[45], viruses[46], long synthetic nanorods[47], or DNA oligonucleotides[48]. This calls for an extension of the presented theory beyond a dumbbell to particles composed of many beads, which is the subject of our ongoing work.

Thus, a meaningful comparison requires measurements of dumbbell-like particles and spherical particles of similar size to determine the shear-viscosity function. Despite our efforts, we could not find satisfactory experiments that would allow such a comparison. We emphasize that this is not a matter of objective difficulties in obtaining such data; rather, it is a matter of probe selection. The essential point is that experiments with all probes (spherical and rod-like) must be performed in the same complex fluid. Usually, in scientific papers, the perspective is one probe in many complex fluids. The methodology described in this paper imposes a different perspective: many probes in one complex fluid. Another possible test of the equations is numerical simulation, which is a topic of ongoing study beyond the scope of this paper.

Therefore, although the methodology outlined above is complete, determining the viscosity function is often cumbersome. Instead of testing the proposed approach by direct comparison with experimental results, we focus on its possible outcomes for the model fluid introduced in this paper via Eq. (21) and for aqueous poly(ethylene glycol) solutions discussed below. To proceed, we use a recently proposed phenomenological relation between the self-mobility of a bead and the viscosity function[14],

$$\mu_{\mathrm{single}}(a) \approx \frac{1}{3\pi^2}\int_0^{\infty} \mathrm{d}k\, \frac{j_0(ka)}{\eta(k)}. \tag{27}$$

This expression leads to simple formulas for the effective Green function. In particular, inserting Eq. (18) into the above integral yields the positional component

$$\phi(R) \approx \mu_{\mathrm{single}}(R), \tag{28}$$

so that $\phi(R)$ is directly expressed through the self-mobility of a spherical particle of radius R. The second

View Article Online
DOI: 10.1039/D6SM00101G

component $\psi(R)$ then follows from Eq. (20).

Applying this phenomenological scheme to the viscosity function in Eq. (21) produces Eqs. (22) and (23) for $\phi(R)$ and $\psi(R)$. With these ingredients, the "point-force coupling" approximation defined by Eq. (15) directly yields the parallel and perpendicular mobilities of the dumbbell.

Equation (22) contains an exponential term, and $\phi(R)$ decreases monotonically with increasing R. A monotonicity analysis of Eq. (23) shows that $\psi(R)$ increases monotonically toward zero from below; hence, $\psi(R) < 0$ for all $R > 0$. Using Eq. (26), this immediately implies that the parallel mobility always exceeds the perpendicular mobility, $\mu_\parallel > \mu_\perp$. Furthermore, if both mobility coefficients are positive - as required physically - their ratio necessarily satisfies $\mu_\parallel/\mu_\perp > 1$.

The dumbbell mobility depends on four parameters a, R, $\eta_{\text{macro}}/\eta_0$, and λ. The first two characterize the dimer, while the latter two characterize the viscosity function of the complex fluid. Fig. 2 shows the mobility ratio curves for a dimer composed of two identical spherical beads of radius $a = 10^{-8}$ m, separated by a center-to-center distance $R = 3a$ and $R = 6a$. In our calculations, the macroscopic viscosity was varied over the range $\eta_{\text{macro}}/\eta_0 \in [1, 10^5]$. The length λ spanned values from $10^{-3}\,\mu$m to $10^2\,\mu$m, corresponding to different complex fluids. For a dimer with $R = 3a$ and $a = 0.01\,\mu$m, with $\lambda \in [0.001, 100]\,\mu$m we observe an increase of the mobility ratio with $\eta_{\text{macro}}/\eta_0$, which sometimes reaches a large ratio $\mu_\parallel/\mu_\perp \gg 1$. In this case, the parallel motion of the dumbbell significantly exceeds the perpendicular mobility, resembling reptation-like motion of a polymer moving between immobile obstacles[29]. Such reptation-like behavior can already be anticipated from the effective Green function itself: as shown in Fig. 1b, the velocity field at distances of order 0.5μm from the point force exhibits regions of upward flow that effectively slow transverse motion of the dumbbell. We note that reptation-like behavior may also arise from structural features of complex fluids and direct interactions, which, though important, are not the focus of the present work. We performed the same analysis for a dimer with $R = 6a$. While for $\lambda = 0.001\,\mu$m the mobility ratio increases, for $\lambda = 0.01\,\mu$m we observe a decrease of $\mu_\parallel/\mu_\perp$, signaling nearly isotropic, sphere-like motion of the dimer.

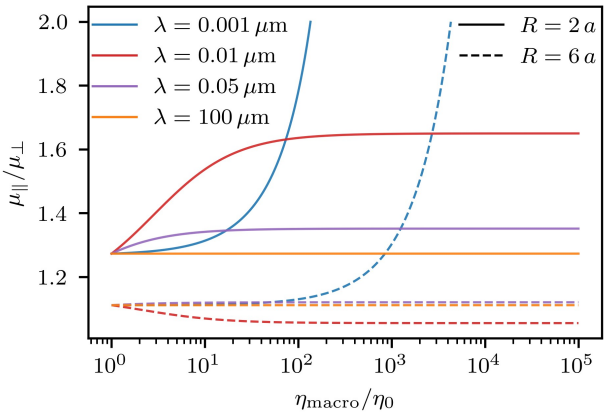

Figure 2: Mobility ratio $\mu_\parallel/\mu_\perp$ for a dimer composed of two identical spherical beads of radius $a = 10^{-8}$ m, separated by a center-to-center distance R. The mobility coefficients are determined by the "point-force coupling" approximation defined by Eq. (15) in the complex fluid with the viscosity function from Eq. (21) characterized by macroscopic-to-solvent viscosity ratio $\eta_{\text{macro}}/\eta_0$ and length λ [μm]. The single-bead mobilities required in the "point-force coupling" approximation were determined from Eq. (28).

4.1 Predictions for poly(ethylene glycol) solutions

We further determined the mobility of a dumbbell in aqueous polymer solutions containing linear poly(ethylene glycol) chains of molecular weight M_w and concentration c[49]. In these polymer solutions, phenomenological formulas for the probe diffusivity as a function of probe radius, $\mu_{\text{single}}(a)$, are available (see Eqs. (4-7) in Ref.[49], which we use with parameters $b = 0.24$, $\beta = -0.75$, $\alpha = 0.62$; notation as in Ref.[49]).

More specifically, experimental data on the mobility of different probes in PEG solutions are represented in terms of the nanoviscosity $\eta_n(a)$, an auxiliary quantity defined by

$$\eta_n(a) = \frac{1}{6\pi a \mu_{\text{single}}(a)}. \tag{29}$$

According to these findings, the nanoviscosity is modeled as

$$\eta_n(a) = \eta_0 \exp\left[\left(\frac{R_{\text{eff}}(a)}{\xi_{PEG}}\right)^{\alpha}\right], \tag{30}$$

where α is the PEG exponential constant, with value 0.62[49]; η_0 is the viscosity of water; and $R_{\text{eff}}(a)$ is an effective hydrodynamic radius that combines the probe radius a and the polymer hydrodynamic radius R_h via

$$R_{\text{eff}}^{-2} = R_h^{-2} + a^{-2}, \tag{31}$$

with

$$R_h = 0.0145\left(\frac{M_w}{g/mol}\right)^{0.57} nm = \rho_1\left(\frac{M_w}{g/mol}\right)^{\rho_{1e}} nm, \tag{32}$$

where M_w is the molecular weight of PEG chains in solution. The PEG correlation length, ξ_{PEG}, is defined as

$$\xi_{PEG} = bR_g\left(\frac{c}{c^*}\right)^{\beta}, \tag{33}$$

where $b = 0.24$[49]. The exponent β depends on solvent type; we use $\beta = -0.75$ for a good solvent[50]. Here, c is the PEG concentration, and c^* is the overlap concentration given by

$$c^* = \frac{M_w}{1.33\pi R_g^3 N_A}, \tag{34}$$

View Article Online
DOI: 10.1039/D6SM00101G

where

$$R_g = 0.0215 \left(\frac{M_w}{g/mol}\right)^{0.58} \text{nm} = \rho_2 \left(\frac{M_w}{g/mol}\right)^{\rho_{2e}} nm. \tag{35}$$

The macroscopic viscosity of the complex fluid is the nanoviscosity in the limit of large probe hydrodynamic radii:

$$\eta_{\text{macro}} = \lim_{a\to\infty} \eta_n(a). \tag{36}$$

Using Eq. (30) in Eq. (36), we obtain the following expression for the macroscopic viscosity:

$$\eta_{\text{macro}} = \eta_0 \exp\left[\left(\frac{R_h}{\xi_{PEG}}\right)^{\alpha}\right]. \tag{37}$$

Following[49] and using Eqs. (32), (33), 34, (35), and (37), we obtain a formula for PEG concentration in terms of M_w and macroscopic viscosity η_{macro}:

$$c = \omega \left(\frac{M_w}{g/mol}\right)^{\varepsilon} \left[\frac{1}{log\left(\eta_{\text{macro}}/\eta_0\right)}\right]^{\gamma} g/L, \tag{38}$$

where $\gamma = \frac{1}{\alpha_{PEG}\beta}$, $\epsilon = 1 + \frac{\rho_{1e}-\rho_{2e}}{\beta} - 3\rho_{2e}$, $\overline{\omega} = \frac{1}{\frac{4}{3}\pi N_A \rho_2^3}\left(\frac{\rho_1}{b\rho_2}\right)^{1/\beta}$ 1/mol, and $\omega = \overline{\omega}\times 10^{24}$. For the PEG parameter values adopted above, we obtain $\omega = 10059$, $\varepsilon = -0.727$, and $\gamma = -2.15$.

The above formulas allow us to determine the probe mobility, $\mu_{\text{single}}(a)$, in PEG with a chosen macroscopic viscosity η_{macro} and molecular weight M_w. Applying these formulas in Eq. (28), together with Eqs. (20), (24), and (25), yields the dumbbell's parallel and perpendicular diffusivities.

We performed calculations for polymer solutions with macroscopic viscosities $\eta_{\text{macro}}/\eta_0 \in [1, 10^5]$, molecular weights $M_w = \{325, 3461, 10944, 15040, 276862, 2000000\}$ g/mol, and the single-bead radius $a = 0.01\,\mu$m and dumbbell size $R = 3a, 6a$. These calculations in poly(ethylene glycol) lead to the same conclusions as for the complex fluid described by the phenomenological relation in Eq. (21): depending on the PEG concentration c, molecular weight M_w, a point force generates a velocity field without (as in Fig. 1a) and with (as in Fig. 1b) vortex-like structures. Moreover, the diffusion of a dumbbell is either isotropic ($\mu_\parallel/\mu_\perp \approx 1$) or resembles reptation-like motion ($\mu_\parallel/\mu_\perp \gg 1$), similarly to the behavior shown in Fig. 2.

5 Conclusions

We have examined the diffusion of rod-like particles in complex fluids using an approximation motivated by recent statistical-mechanical insights into Smoluchowski dynamics. The key ingredients of the approach are the mobility of a single spherical bead and the wave-vector-dependent viscosity $\eta(k)$, which encodes dissipation across length scales. Within this framework, the parallel and perpendicular mobilities of a dimer follow from a simple expression involving the effective Green function of the fluid.

This minimal description captures the full range of behaviors observed for rod-like probes, from nearly isotropic, sphere-like motion to strongly anisotropic, reptation-like dynamics. Because the approximation depends only on μ_{single} and $\eta(k)$, it can be applied broadly in experiments and simulations whenever these quantities are known, without introducing additional phenomenological parameters.

The range of conditions under which the hydrodynamic contribution considered here dominates remains an open question. Clarifying these limits will require further analysis.

Conflicts of interest

There are no conflicts of interest to declare.

Acknowledgments

W.S., H.J. and K.M. acknowledge support from the National Science Centre, Poland, under Grant No. 2021/42/E/ST3/00180. We thank Zhen-Gang Wang and Alexandros Tsamopoulos for valuable discussions.

References

[1] Youssef Habibi, Lucian A. Lucia, and Orlando J. Rojas. Cellulose nanocrystals: Chemistry, self-assembly, and applications. *Chemical Reviews*, 110(6):3479–3500, 2010. PMID: 20201500.

[2] J. Howard. Mechanics of motor proteins and the cytoskeleton. *Applied Mechanics Reviews*, 55(2):B39–B39, 04 2002.

[3] Sean Michael Kerwin. Nucleic acids: Structures, properties, and functions. *Journal of Medicinal Chemistry*, 43(24):4721–4722, 2000. Review of the book by Bloomfield, Crothers, and Tinoco.

[4] Masao Doi. *Soft matter physics*. Oxford University Press, 2013.

[5] F. Brochard Wyart and P. G. de Gennes. Viscosity at small scales in polymer melts. *The European Physical Journal E*, 1(1):93–97, 2000.

[6] Denis J Evans and Gary Morriss. *Statistical Mechanics of Nonequilibrium Liquids*. Cambridge University Press, 2008.

[7] U Balucani, R Vallauri, and T Gaskell. Transverse current and generalized shear viscosity in liquid rubidium. *Physical Review A*, 35(10):4263, 1987.

View Article Online
DOI: 10.1039/D6SM00101G

[8] C.W.J. Beenakker. The effective viscosity of a concentrated suspension of spheres (and its relation to diffusion). *Physica A: Statistical Mechanics and its Applications*, 128(1):48–81, 1984.

[9] Piotr Szymczak and Bogdan Cichocki. A diagrammatic approach to response problems in composite systems. *Journal of Statistical Mechanics: Theory and Experiment*, 2008:P01025, 2008.

[10] T Gaskell, U Balucani, M Gori, and R Vallauri. Wavevector-dependent shear viscosity in lennard-jones liquids. *Physica scripta*, 35(1):37, 1987.

[11] JS Hansen, Peter J Daivis, Karl P Travis, and BD Todd. Parameterization of the nonlocal viscosity kernel for an atomic fluid. *Physical Review E—Statistical, Nonlinear, and Soft Matter Physics*, 76(4):041121, 2007.

[12] Kirill S Glavatskiy, Benjamin A Dalton, Peter J Daivis, and BD Todd. Nonlocal response functions for predicting shear flow of strongly inhomogeneous fluids. i. sinusoidally driven shear and sinusoidally driven inhomogeneity. *Physical Review E*, 91(6):062132, 2015.

[13] RM Puscasu, BD Todd, PJ Daivis, and Jesper Schmidt Hansen. Viscosity kernel of molecular fluids: Butane and polymer melts. *Physical Review E*, 82(1):011801, 2010.

[14] Karol Makuch, Robert Hołyst, Tomasz Kalwarczyk, Piotr Garstecki, and John F. Brady. Diffusion and flow in complex liquids. *Soft Matter*, 16:114–124, 2020.

[15] M Muthukumar. Viscosity of polymer solutions. *Journal of Physics A: Mathematical and General*, 14(8):2129, 1981. Pre-average approximation.

[16] W Hess. Wave vector and frequency dependent longitudinal viscosity of systems of interacting brownian particles. *Physica A Statistical Mechanics and its Applications*, 107(1):190–200, 1981.

[17] MW Heemels, CP Lowe, and AF Bakker. The wavelength dependence of the high-frequency shear viscosity in a colloidal suspension of hard spheres. *Trends in Colloid and Interface Science XII*, pages 150–155, 2008.

[18] RM Puscasu, BD Todd, Peter J Daivis, and Jesper Schmidt Hansen. Nonlocal viscosity of polymer melts approaching their glassy state. *The Journal of chemical physics*, 133(14):144907, 2010.

[19] Alexander Y Grosberg, Jean-François Joanny, Watee Srinin, and Yitzhak Rabin. Scale-dependent viscosity in polymer fluids. *The Journal of Physical Chemistry B*, 2016.

[20] Siegfried Hess. Fokker-planck-equation approach to flow alignment in liquid crystals. *Zeitschrift für Naturforschung A*, 31(9):1034–1037, 1976.

[21] Masao Doi. Molecular dynamics and rheological properties of concentrated solutions of rodlike polymers in isotropic and liquid crystalline phases. *Journal of Polymer Science: Polymer Physics Edition*, 19(2):229–243, 1981.

[22] T Keyes and Irwin Oppenheim. Bilinear hydrodynamics and the stokes-einstein law. *Physical Review A*, 8(2):937, 1973.

[23] T Keyes. Self-diffusion in a binary critical fluid. *The Journal of Chemical Physics*, 62(5):1691–1692, 1975.

[24] Joohyun Kim and T Keyes. On the breakdown of the stokes- einstein law in supercooled liquids. *The Journal of Physical Chemistry B*, 109(45):21445–21448, 2005.

[25] Umi Yamamoto and Kenneth S Schweizer. Theory of nanoparticle diffusion in unentangled and entangled polymer melts. *The Journal of chemical physics*, 135(22):224902, 2011.

[26] Jeffrey C Everts, Robert Hołyst, and Karol Makuch. Brownian motion at various length scales with hydrodynamic and direct interactions. *Physics of Fluids*, 37(2), 2025.

[27] Julie L Bitter, Yuguang Yang, Gregg Duncan, Howard Fairbrother, and Michael A Bevan. Interfacial and confined colloidal rod diffusion. *Langmuir*, 33(36):9034–9042, 2017.

[28] Jia Zhang, Lijun Yang, Hai-Xing Wang, Jiuling Wang, and Ruo-Yu Dong. Cross-sectional effects on nanorod diffusion in polymer melts. *Macromolecules*, 58(10):4959–4970, 2025.

[29] Pierre-Giles De Gennes. Reptation of a polymer chain in the presence of fixed obstacles. *The journal of chemical physics*, 55(2):572–579, 1971.

[30] Richard M Jendrejack, Juan J de Pablo, and Michael D Graham. Stochastic simulations of dna in flow: Dynamics and the effects of hydrodynamic interactions. *The Journal of chemical physics*, 116(17):7752–7759, 2002.

[31] Martin Kröger. Simple models for complex nonequilibrium fluids. *Physics reports*, 390(6):453–551, 2004.

[32] Manuel Quesada-Pérez and Alberto Martín-Molina. Solute diffusion in gels: Thirty years of simulations. *Advances in Colloid and Interface Science*, 287:102320, 2021.

View Article Online
DOI: 10.1039/D6SM00101G

[33] Brian Amsden. Solute diffusion within hydrogels. mechanisms and models. *Macromolecules*, 31(23):8382–8395, 1998.

[34] Mohammad-Reza Rokhforouz, Don D Sin, Sarah Hedtrich, and James J Feng. Brownian dynamics simulation of the diffusion of rod-like nanoparticles in polymeric gels. *Soft Matter*, 21(27):5529–5541, 2025.

[35] Marian Smoluchowski. On the practical applicability of stokes' law of resistance and its modifications required in certain cases. *Pisma Mariana Smoluchowskiego*, 2(1):195–208, 1927.

[36] S. Kim and S.J. Karrila. *Microhydrodynamics: Principles and Selected Applications*. Butterworth-Heinemann Boston, 1991.

[37] Donald L. Ermak and J. A. McCammon. Brownian dynamics with hydrodynamic interactions. *The Journal of Chemical Physics*, 69(4):1352–1360, 08 1978.

[38] Yilong Han, Ahmed M Alsayed, Maurizio Nobili, Jian Zhang, Tom C Lubensky, and Arjun G Yodh. Brownian motion of an ellipsoid. *Science*, 314(5799):626–630, 2006.

[39] J.K.G. Dhont. *An introduction to dynamics of colloids*. Elsevier, 2003.

[40] B. Cichocki, ML Ekiel-Jeżewska, P. Szymczak, and E. Wajnryb. Three-particle contribution to sedimentation and collective diffusion in hard-sphere suspensions. *The Journal of Chemical Physics*, 117:1231, 2002.

[41] Karol Makuch. Generalization of clausius-mossotti approximation in application to short-time transport properties of suspensions. *Phys. Rev. E*, 92:042317, Oct 2015.

[42] Maciej Lisicki. Four approaches to hydrodynamic green's functions – the oseen tensors, 2013.

[43] Andrej Vilfan, Bogdan Cichocki, and Jeffrey C. Everts. Stokes drag on a sphere in a three-dimensional anisotropic porous medium, 2025.

[44] Venkat Ganesan, Victor Pryamitsyn, Megha Surve, and Bharadwaj Narayanan. Noncontinuum effects in nanoparticle dynamics in polymers. *The Journal of chemical physics*, 124(22):221102, 2006.

[45] Farshad Safi Samghabadi, Juexin Marfai, Camyla Cueva, Mehdi Aporvari, Philip Neill, Maede Chabi, Rae M Robertson-Anderson, and Jacinta C Conrad. Phage probes couple to dna relaxation dynamics to reveal universal behavior across scales and regimes. *Soft matter*, 21(5):935–947, 2025.

[46] Randy Cush, Paul S Russo, Zuhal Kucukyavuz, Zimei Bu, David Neau, Ding Shih, Savas Kucukyavuz, and Holly Ricks. Rotational and translational diffusion of a rodlike virus in random coil polymer solutions. *Macromolecules*, 30(17):4920–4926, 1997.

[47] Jihoon Choi, Matteo Cargnello, Christopher B Murray, Nigel Clarke, Karen I Winey, and Russell J Composto. Fast nanorod diffusion through entangled polymer melts. *ACS Macro Letters*, 4(9):952–956, 2015.

[48] A Wilk, J Gapinski, Adam Patkowski, and R Pecora. Self-diffusion in solutions of a 20 base pair oligonucleotide: effects of concentration and ionic strength. *The Journal of chemical physics*, 121(21):10794–10802, 2004.

[49] Tomasz Kalwarczyk, Natalia Ziębacz, Anna Bielejewska, Ewa Zaboklicka, Kaloian Koynov, Jędrzej Szymański, Agnieszka Wilk, Adam Patkowski, Jacek Gapiński, Hans-Jürgen Butt, and Robert Hołyst. Comparative analysis of viscosity of complex liquids and cytoplasm of mammalian cells at the nanoscale. *Nano Letters*, 11(5):2157–2163, 2011. PMID: 21513331.

[50] Yu Cheng, Robert K Prud'Homme, and James L Thomas. Diffusion of mesoscopic probes in aqueous polymer solutions measured by fluorescence recovery after photobleaching. *Macromolecules*, 35(21):8111–8121, 2002.

View Article Online
DOI: 10.1039/D6SM00101G

Data availability statement

Data availability. This work is theoretical and does not report new experimental measurements or simulation datasets. All results can be reproduced from the equations and parameters provided in the manuscript. No additional data are associated with this article.